land

MDPI

Article

Groundwater Potential Zones Assessment Using Geospatial Models in Semi-Arid Areas of South Africa

Gbenga Olamide Adesola [1,*], Kgabo Humphrey Thamaga [2], Oswald Gwavava [1] and Benedict Kinshasa Pharoe [1]

[1] Department of Geology, University of Fort Hare, 1 King William's Town Road, Alice 5700, South Africa; ogwavava@ufh.ac.za (O.G.); bpharoe@ufh.ac.za (B.K.P.)
[2] Department of GIS and Remote Sensing, University of Fort Hare, 1 King William's Town Road, Alice 5700, South Africa; kthamaga@ufh.ac.za
* Correspondence: gbengaadesola@gmail.com

Abstract: Water resources are under tremendous pressure as a result of the growing demand for water to meet human needs. Hence, it is necessary to delineate groundwater potential zones (GWPZs) to sustainably develop and manage groundwater resources. In this study, the geospatial-based analytical hierarchy process (AHP) and frequency ratio (FR) techniques were used to identify the GWPZs. Seven factors (geology, rainfall, slope, lineament density, soil, drainage density, and land use/land cover), which partially or entirely influence the groundwater potentiality of an area, were accessed separately and later combined to create GWPZ maps. Weights and ranks were assigned to the factors to perform the AHP model using existing knowledge. The FR was performed by calculating the percentage ratio between the dependent variable (boreholes) and the independent variable (factors). The preparation of the contributing factors and the creation of the resulting models was done using ArcGIS 10.8. The final GWPZ maps were classified into five zones: very low, low, moderate, high, and very high. About 80 boreholes in the study area were randomly subset into training and testing datasets; 58% were used for model training, and the remaining 42% were used for validation purposes. The receiver operating characteristic (ROC) curves for the GWPZs models were generated, and the areas under the curves (AUC) were calculated. Validation of the models shows that the FR model is more efficient (85.3% accuracy) than the AHP model (83.2% accuracy). The findings show that the AHP and FR models are reliable and can be adopted to characterize GWPZs in arid or semi-arid environments.

Keywords: GIS; groundwater; frequency ratio; ROC; water scarcity

Citation: Adesola, G.O.; Thamaga, K.H.; Gwavava, O.; Pharoe, B.K. Groundwater Potential Zones Assessment Using Geospatial Models in Semi-Arid Areas of South Africa. *Land* **2023**, *12*, 1877. https://doi.org/10.3390/land12101877

Academic Editor: Frédéric Frappart

Received: 28 August 2023
Revised: 29 September 2023
Accepted: 3 October 2023
Published: 6 October 2023

1. Introduction

Groundwater is a significant source of freshwater on the surface of the earth [1]. The availability and flow of groundwater are influenced by geological units, lineament density, slope, soil type, land use land cover, rainfall characteristics, and drainage density, as well as their relationships with each other [2]. Globally, groundwater is used for drinking, irrigation, industrial and other uses [3,4]. Groundwater consumption is more reliable and fresher than surface water as groundwater is less susceptible to disastrous occurrences (i.e., surface contaminations and pollution than surface water) on the earth's surface [5]. Excessive groundwater withdrawal has resulted in decreasing groundwater levels and rising pressure on existing groundwater resources in various regions of the world due to the growing rate of development, insufficient rainfall, and agricultural expansion worldwide to cater to rising energy demands and global food security [6–8]. Rapid population growth, urbanization, industrialization, and the severe aridity of water resources in South Africa, further exacerbated by climate change, water scarcity may last longer [9]. The Eastern Cape Province in South Africa suffers from critical water scarcity [10–12]. Following severe water shortages in numerous urban and rural areas, the Eastern Cape Province was classified

as a drought disaster province in October 2019 [12]. Identifying groundwater potential zones is one of the keys to resolving water problems worldwide. Lately, efforts to identify groundwater potential zones have been increasing globally [13]. Thus, there is a need for frequent and accurate mapping and understanding of the available groundwater resources at a larger scale.

Over the years, several conventional methods, such as geological, geophysical, and hydrogeological, have been used to identify and explore GWPZ [14–16]. Various geophysical methods, such as electromagnetic, seismic refractive, gravity, magnetic, and electrical resistivity techniques, have been utilized in geophysics to explore groundwater [17–21]. These geophysical methods usually require deep penetration to evaluate the geological components that are potential groundwater indicators. The electrical resistivity and electromagnetic methods have been proven to be effective compared to other geophysical methods [22–24]. Nevertheless, these approaches are constrained by demanding field work, complicated and expensive instruments, time-consuming, and in-depth knowledge of different aquifer types [25]. Given these limitations, assessing groundwater resources using advanced techniques such as remote sensing (RS) and geographic information systems (GIS) is essential.

Numerous researchers have successfully used RS and GIS methods globally to process factors that control groundwater for identifying groundwater potential zones (GWPZ) in the GIS environment [18,26–28]. The significant benefits of RS and GIS methods have also been recognized in enhancing our capacity to investigate groundwater resources on a regional scale [29]. The input factors characterizing the potential of the groundwater in a region can be assessed, processed, and integrated within the GIS environment to produce a final GWPZ map [30]. The use of various groundwater influencing factors varies from one study to another and with the availability of data. However, many studies have been conducted worldwide using various multi-criteria decision-making analysis and machine learning algorithms with differing accuracy to identify GWPZs and carry out mapping [31–34]. Among these methods, the knowledge-driven analytic hierarchy process (AHP) model is the common method several researchers employ to assess and map GWPZ [4,15,28,35–37]. The AHP and geospatial techniques were used by [4] to identify GWPZs in Precambrian hard rock terranes (North Gujarat), India, and noted that the AHP requires pairwise comparison, existing literature, and expert knowledge to assign weights to different groundwater influencing factors. Also, [35] successfully assessed GWPZs in the coal mining area impacted hard-rock terrain of India using integrated geospatial and AHP approaches. The limitation of AHP is related to its dependency on the expert's knowledge which is the primary source of uncertainty [38]. Although not as commonly used as AHP, the data-driven frequency ratio (FR) model has been used by various researchers to evaluate spatial relationships between the dependent variable (boreholes) and the independent variables (groundwater controlling factors) in mapping GWPZ [39–41]. A comparison assessment between FR and AHP techniques for GWPZ mapping in the Vaitarna basin, India, was carried out by [40], and reported that the FR model is more efficient (75% accuracy) than the AHP technique (70% accuracy).

Recently, some modern techniques have been used by various researchers for groundwater exploration, among which the weights-of-evidence model [42–44]; logistic model tree [45]; fuzzy-gamma [46]; Dempster-Shafer model [47]; logistic regression [48]; Shannon's entropy [49]; random forest model [50]; maximum entropy model [51]; decision tree model [52]; evidential belief function [26]; artificial neural network [53] have been successfully implemented. The AHP and FR methods have gained popularity among other techniques because they offer a versatile, affordable, less time-consuming, and simple method for analyzing challenging issues regarding groundwater resources in particular [28,35,54].

The Buffalo City Metropolitan Municipality (BCMM) residents are supplied with piped water by the Amatole Water Supply System (AWSS) [11]. The abstraction of water resources for various purposes occurs at the municipality's dam sites [55]. However, these water sources would generally be inadequate to meet the region's water needs by the end

of the present decade due to economic growth, aging municipal water infrastructure, and population [56]. According to regional studies [57,58], increasing temperatures and an increase in the frequency of catastrophic occurrences, such as droughts, are anticipated to significantly diminish the future dependability of the region's surface water supplies. The exploitation of groundwater resources as a substitute for surface water has not been fully utilized due to a lack of information on their development [59]. Groundwater can be a dependable and affordable water source, and its contribution to diversifying water supply sources merits further investigation in water-stressed areas [60]. The distribution of groundwater is still not well understood in BCMM [61]. Despite being a highly water-stressed area, the use of RS and GIS techniques to understand groundwater distribution is few in this area. As a result, there is a need for the effective execution of strategies to manage groundwater resources through monitoring groundwater exploitation to minimize the effect of water scarcity in the study area [62]. Therefore, the paper aims to address the gap in the comprehensive investigation of groundwater potential in the study area, raise awareness of groundwater availability, offer regional approaches to delineate GWPZ using integrated multi-criteria analysis (GIS-based AHP and FR models), and compare the models in evaluating their proficiency in deciphering groundwater potentiality, as a means of achieving the goal of water sustainability. Moreover, the study shows the importance of the AHP and FR models for preparing an efficient and low-cost approach for delineating GWPZs, which may also be applied in other semi-arid environments. The approach developed in this study would be of tremendous benefit to the decision-makers, stakeholders, and the host community at large.

2. Materials and Methods

2.1. Study Area

The BCMM is located on the east coast of Eastern Cape Province (Figure 1), situated between latitudes 32°34′40″ S to 33°12′0″ S and longitudes 27°10′54.15″ E to 27°17′26.43″ E. It covers a total area of about 2 536 km^2, with a maximum elevation of about 1 352 m above sea level (a.s.l). BCMM includes the major towns of East London, Qonce, Bisho, Berlin, Mdantsane, and Dimbaza. The population of BCMM is estimated at 755,200 [63]. The main rivers in BCMM include the Buffalo, Yellowwoods, and Nahoon Rivers. The mean annual rainfall varies between 692 and 850 mm; the mean annual temperature ranges between 16–23 °C [11]. The vegetation consists mainly of indigenous forests, pine, and blue gum plantations [64]. Geologically, the study area falls within the Karoo Supergroup. The study area is geologically dominated by Adelaide and Tarkastad Subgroups of the Beaufort Group, which are intruded by Jurassic dolerites (sills and dykes) [65]. Most aquifers have groundwater discharge of less than 5 l/s [66].

2.2. Data Sources

This study combined several groundwater controlling factors, including lineament density, rainfall, drainage density, lithology, soil type, land use/land cover (LULC), and slope from various sources to delineate GWPZs. The Shuttle Radar Topography Mission Digital Elevation Model (SRTM DEM) of 30 m spatial resolution was obtained from Open Topography (https://www.opentopography.org (accessed on 3 July 2023)). Firstly, DEM was filled to generate a drainage density map. An accurate drainage map was produced using ArcGIS 10.8's flow direction and flow accumulation commands afterward. The raster drainage map was converted to vector format using the conversion tools. Lastly, the line density tool in the ArcGIS 10.8 software command was employed to create the drainage density map. The spatial analyst slope tool in the ArcGIS 10.8 software was employed to generate the slope map. The LULC data for the year 2022 was obtained from the Sentinel-2 (10 m cell size) source imagery of the Environmental Systems Research Institute (ESRI). A 1:250,000 scale soil data was downloaded from the Soil and Terrain database for South Africa (SOTERSAF) (https://files.isric.org/public/soter/SAF-SOTER.zip (accessed on 3 July 2023)). The South African Weather Service (SAWS) provided rainfall data for the research

area for 22 years (2000–2022), and ArcGIS 10.8 was utilized to produce a mean annual rainfall map with the aid of the Inverse Distance Weighting (IDW) interpolation method.

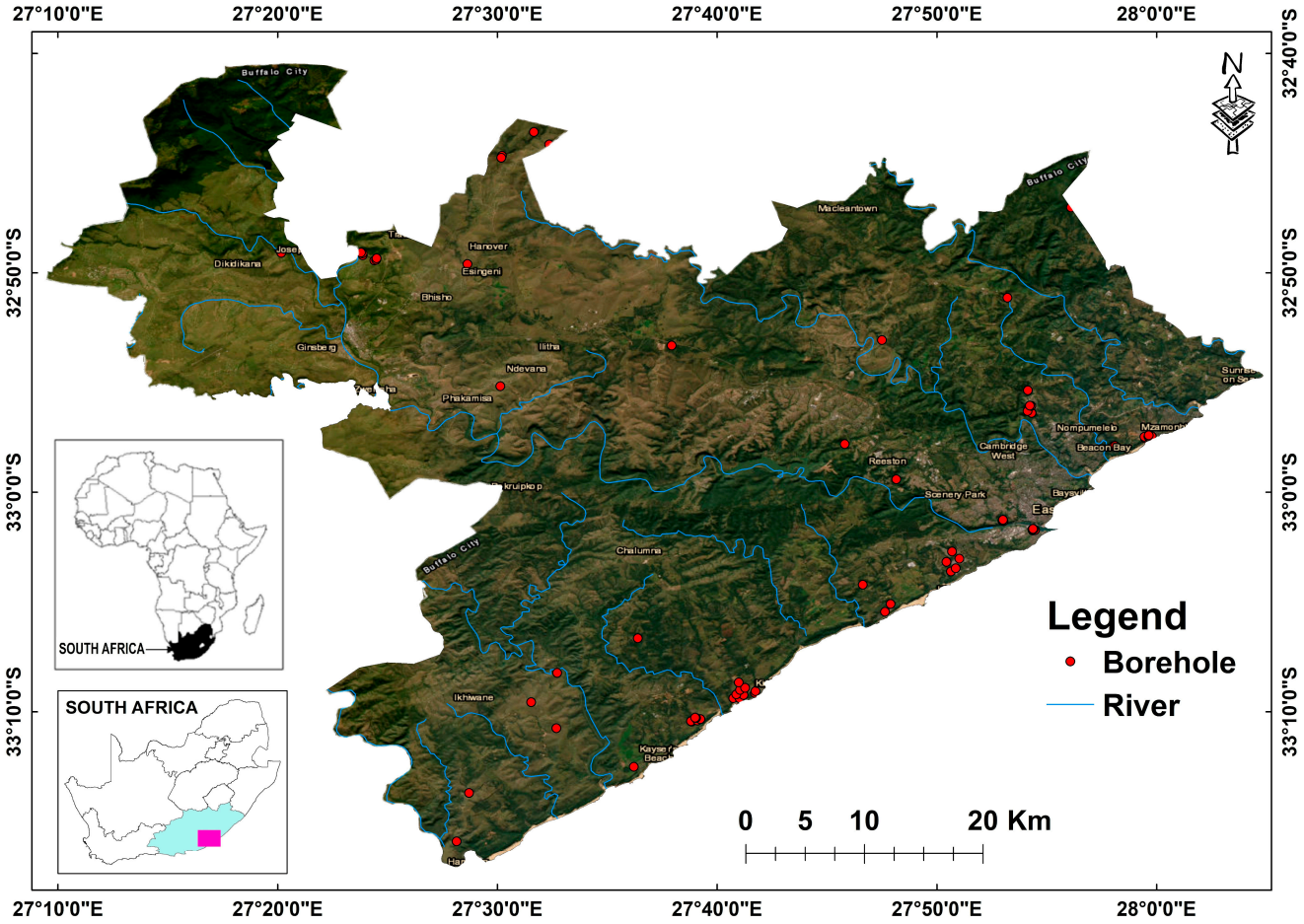

Figure 1. Location of the BCMM in South Africa with its rivers and borehole points.

Cloud-free Landsat-8 data "LC09_L2SP_170083_20220709_20230408_02_T1," dated 9 July 2022, was downloaded from the United States Geological Survey (USGS) website (https://earthexplorer.usgs.gov (accessed on 3 July 2023)) to extract lineament using PCI Geomatica 10.3 automatically. This was accomplished using an algorithm of multi-stage line detection of Canny edge and contour detection [67]. The polylines, referred to as lineaments, are created by these processes. ArcGIS 10.8 software was utilized to process the lineament density. The geology map of the study area was extracted from an existing map of the Geological Survey of South Africa (GSSA) with a scale of 1:250,000 using ArcGIS 10.8 software. The graphical illustration of the data and methods used in this study is shown in Figure 2. Thematic layers were converted to a raster format, reprojected to Universal Transverse Mercator (UTM) Zone 36S, and finally resampled to a 30 × 30 m grid cell.

2.3. Analytical Hierarchy Process (AHP)

AHP combines experts' subjective and rational opinions to achieve decision-making by assessing several factors that influence groundwater potentiality [68]. The AHP model was used to generate the GWPZ map based on the influence of the seven factors (lineament density, soil type, lithology, LULC, rainfall, drainage density, and slope) [54]. This model accelerates the decision-making process through the pairwise comparison matrix of these factors, calculating each factor's weight, the consistency ratio (CR) of the matrix, the GWPZ model, and validation.

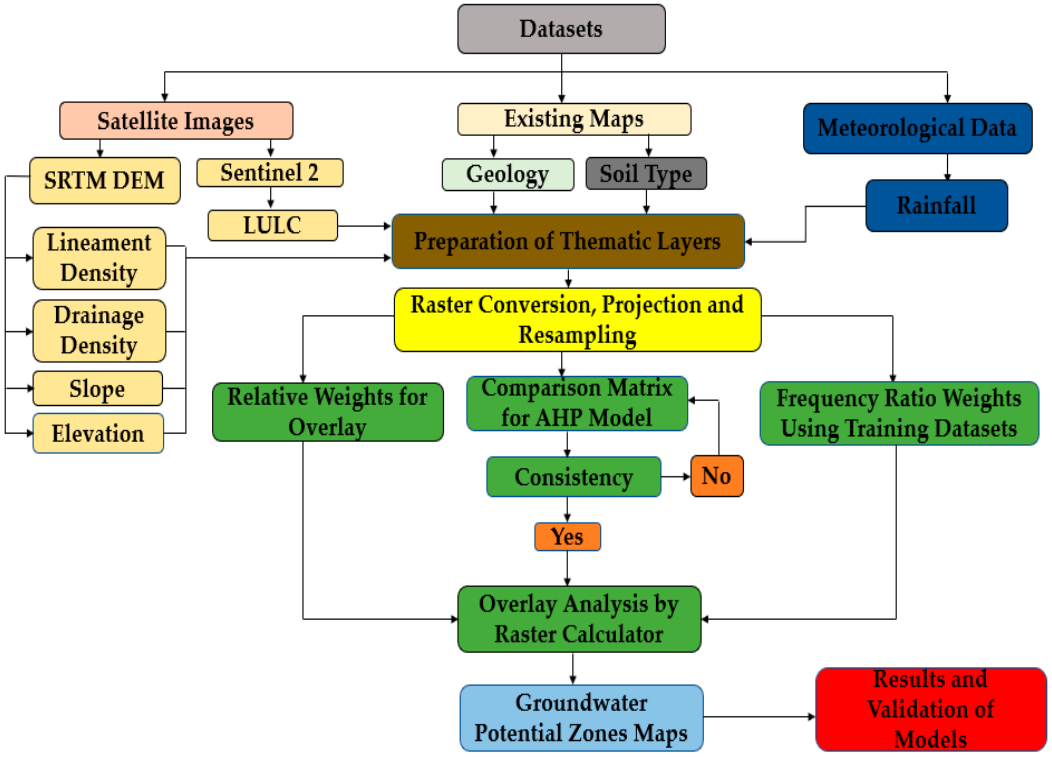

Figure 2. Conceptual framework of the methodology followed in the study.

2.3.1. Pairwise Comparison Matrix and Weighting of Each Groundwater Controlling Factor

The stepwise approach of [54] methodology was adopted in this study. The methodology involves independently evaluating the importance of each factor that influences groundwater potentiality and assigning numeric values for each factor on a scale of 1 (equal significance) to 9 (extreme significance) to obtain the normalized principal eigenvector values (weight of individual factors that control groundwater), as shown in Table 1. Lastly, the accuracy of the pairwise comparison matrix was calculated using CR.

Table 1. Pairwise comparison matrix and weights of groundwater controlling factors.

Matrix		Rainfall	Geology	Slope	Drainage Density	LULC	Lineament Density	Soil	Normalized Principal Eigenvector
		1	2	3	4	5	6	7	
Rainfall	1	1	3	3	5	5	5	7	38.18%
Geology	2	1/3	1	3	3	7	4	5	25.01%
Slope	3	1/3	1/3	1	1	3	3	3	12.11%
Drainage density	4	1/5	1/3	1	1	1	2	3	9.09%
LULC	5	1/5	1/7	1/3	1	1	1	1	5.43%
Lineament density	6	1/5	1/4	1/3	1/2	1	1	3	6.25%
Soil	7	1/7	1/5	1/3	1/3	1	1/3	1	3.94%
							CR = 4.5%		

2.3.2. Consistency Ratio (CR) Calculation

CR is a mathematical indicator of judgment regarding a random decision [13]. The CR value must be less than or equal to 10%, according to [54]. Furthermore, if it comes to greater than 0.1, the assigned values in the pairwise comparison matrix need to be readjusted. The CR is calculated using Equation (1), given by [54].

$$CR = \frac{CI}{RI} \quad (1)$$

CI is the consistency index, and *RI* is the random index. *CI* was calculated using Equation (2):

$$\mathrm{CI} = \frac{\boldsymbol{\lambda_{max}} - \boldsymbol{n}}{\boldsymbol{n} - 1} \quad (2)$$

λ_{max} represents the principal eigenvalue of the matrix, and n is the number of factors.

2.3.3. Groundwater Potential Zone (GWPZ) Model

The groundwater controlling factors were classified into subclasses and were given a rank on a scale of 1 to 5. The most influential subclasses were given a rank score of 5, while the least influential subclasses were assigned a rank score of 1. Finally, The GWPZ map was obtained through the raster calculation in ArcGIS 10.8 software by using Equation (3):

$$GWPZ = \sum_{i=1}^{n}(W_i \times R_i) = (RF_W RF_R + GL_W GL_R + SL_W SL_R + DD_W DD_R + LULC_W LULC_R + LD_W LD_R + ST_W ST_R) \quad (3)$$

W is the weight of each factor, R is the ranking, RF is the rainfall, GL is the geology, SL is the slope, DD is drainage density, LULC is land use/land cover, LD is lineament density, and SC is soil type.

2.4. Frequency Ratio (FR)

The FR is based on the relationship between the distribution of observational boreholes and the groundwater potentiality-related factors [5,27]. The following expression can easily calculate the FR of a certain factor:

$$\mathrm{FR} = \left[\frac{\left(\frac{P_{bh}}{T_{bh}}\right)}{\left(\frac{P_f}{T_f}\right)}\right] = \left[\frac{\boldsymbol{\%bh}}{\boldsymbol{\%pixels}}\right] \quad (4)$$

where, $\boldsymbol{P_{bh}}$ is the number of pixels with boreholes for each parameter, $\boldsymbol{T_{bh}}$ is the number of total boreholes, $\boldsymbol{P_f}$ is the number of pixels in the classes of a parameter, $\boldsymbol{T_f}$ is the total number of pixels of a parameter, and ***bh*** is a borehole.

The FR values of these factors were integrated into ArcGIS 10.8 software and added up to produce the GWPZ map using the following expression:

$$GWPZ_{FR} = \sum(RF_{FR} + GL_{FR} + SL_{FR} + DD_{FR} + LULC_{FR} + LD_{FR} + SC_{FR}) \quad (5)$$

where, $GWPZ_{FR}$ is groundwater potential zones using the frequency ratio technique.

2.5. Borehole Data

The groundwater borehole data were acquired from the BCMM and National Groundwater Archive (NGA) (https://www.dws.gov.za/NGANet/Security/WebLoginForm.aspx, accessed on 10 July 2023)). Eighty (80) active boreholes were randomly subset into two types of datasets (training and testing) using the subset feature method of the geostatistical analyst tool in ArcGIS 10.8. The training dataset used to perform the FR model has 46 boreholes, while the testing data for validating the models had 34 boreholes. The borehole locations are shown in Figure 3.

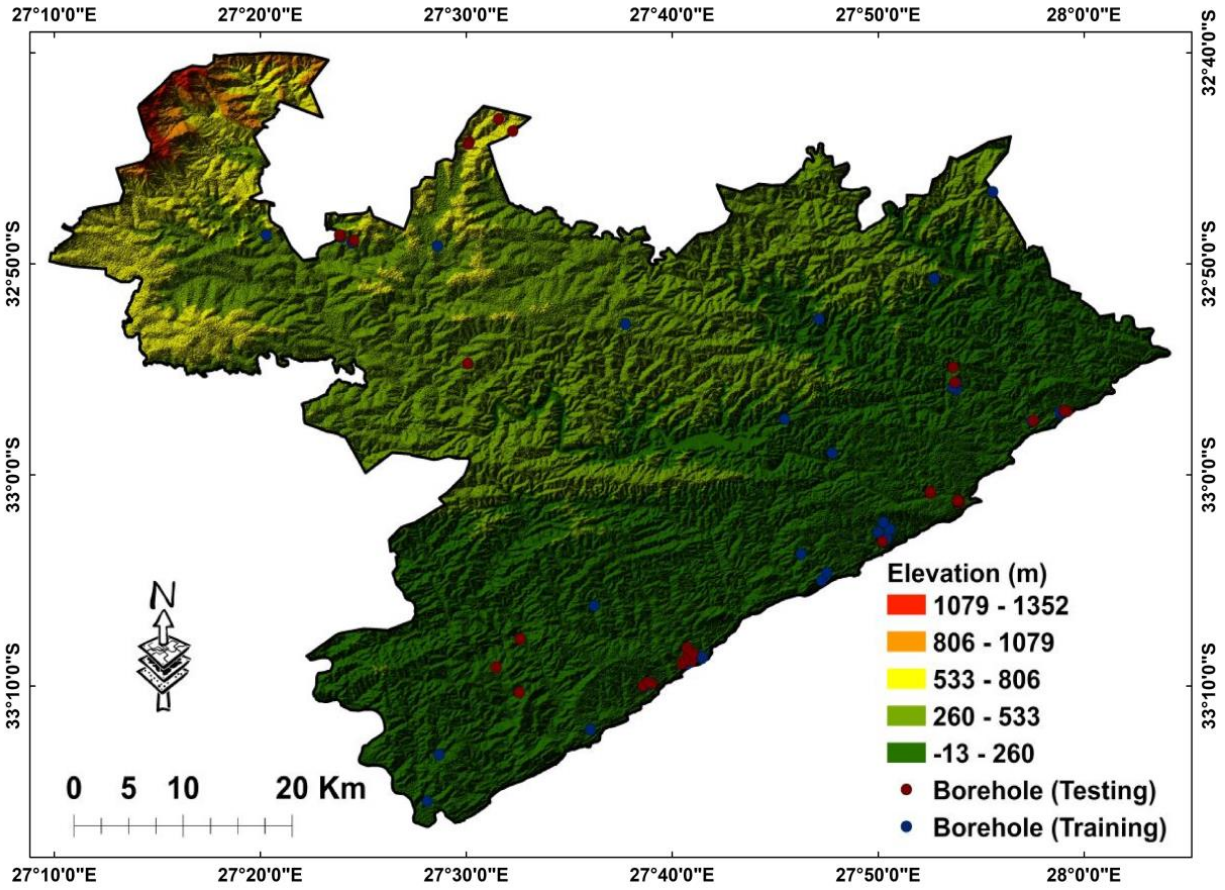

Figure 3. Training and testing boreholes overlayed on the elevation map of the study area.

2.6. Validation of AHP and FR Models

Validating output maps is crucial for determining the accuracy of models, methods, and strategies [69]. Receiver operating characteristic (ROC) curve analysis is a typical methodology to evaluate the accuracy of a model [69]. However, ROC and AUC analyses have been used by several authors to validate GWPZ mapping [5,13,48]. The resultant GWPZ maps from AHP and FR models were validated using the ROC curve. The ArcSDM algorithm embedded in ArcGIS 10.8 was used to generate the AUC values.

3. Results

3.1. Groundwater Controlling Factors

3.1.1. Geology

The geological map of the study area consists of Quaternary sediment (0.93% of the surface area; 10.19 km^2) in the south-eastern part, Nanaga Formation (1.27%; 1.22 km^2) in the southern part, Igoda Formation (0.01%; 0.03 km^2) in the central region, Karoo dolerites (9.38%; 15.60 km^2) in the south-central and north-western parts, Tarkastad Subgroup (6.99%; 1.75 km^2) widely found in the southern part, and Adelaide Subgroup (81.24%; 314.9 km^2), which dominates the study area (Figure 4a). The geological units were ranked based on their influences on groundwater potentiality. Quaternary sediment, Igoda Formation, Tarkastad Supergroup, and Adelaide Supergroup subclass were ranked higher (5) due to their high hydraulic conductivities (Table 2). The Nanaga Formation and Karoo dolerites are the least significant factors for groundwater storage (rank = 4).

3.1.2. Rainfall

The mean annual rainfall of the study area was classified into five subclasses: very low (692–714 mm), low (715–735 mm), moderate (736–757 mm), high (758–778 mm), and very

high (779–850 mm), occupying about 48%, 41%, 7%, 3%, and 1% of the total surface area, respectively (Figure 4b). The generated rainfall map reveals that the area receives very high rainfall in the eastern part, whereas the southwestern and northern parts receive very low to moderate rainfall. In this study, the low rainfall subclass was assigned low ranking and vice versa (Table 2).

3.1.3. Lineament Density

The lineament density map of the study area was classified into the following five subclasses: very low (0–0.0002698 km/km^2), low (0.0002699–0.000549 km/km^2), moderate (0.0005488–0.000873 km/km^2), high (0.0008726–0.001304 km/km^2), and very high (0.0013050–0.002294 km/km^2), occupying approximately 54%, 31%, 10%, 4%, and 1% of the surface area, respectively (Figure 4c). From the lineament density map, the highest lineament density was observed in the central part of the study area. Moderate to high lineament densities were observed in the southwestern and northwest parts. The eastern part of the study area is dominated by very low to low lineament densities. As shown in Table 2, the highest lineament density (0.0013050–0.002294 km/km^2) was assigned the maximum rank (5), and the lowest rank (1) was assigned to the lineament density class of 0–0.0002698 km/km^2 (Table 2).

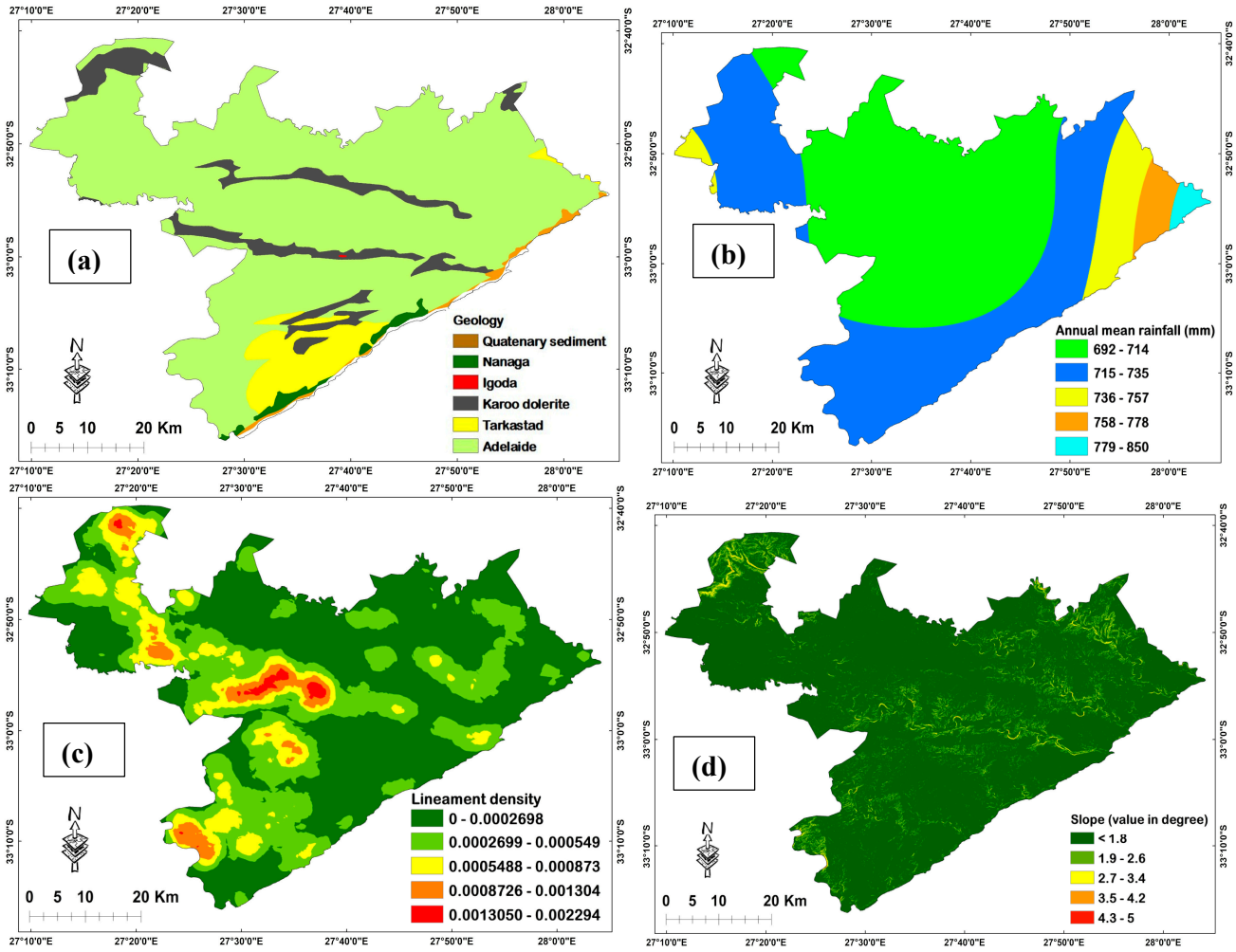

Figure 4. *Cont.*

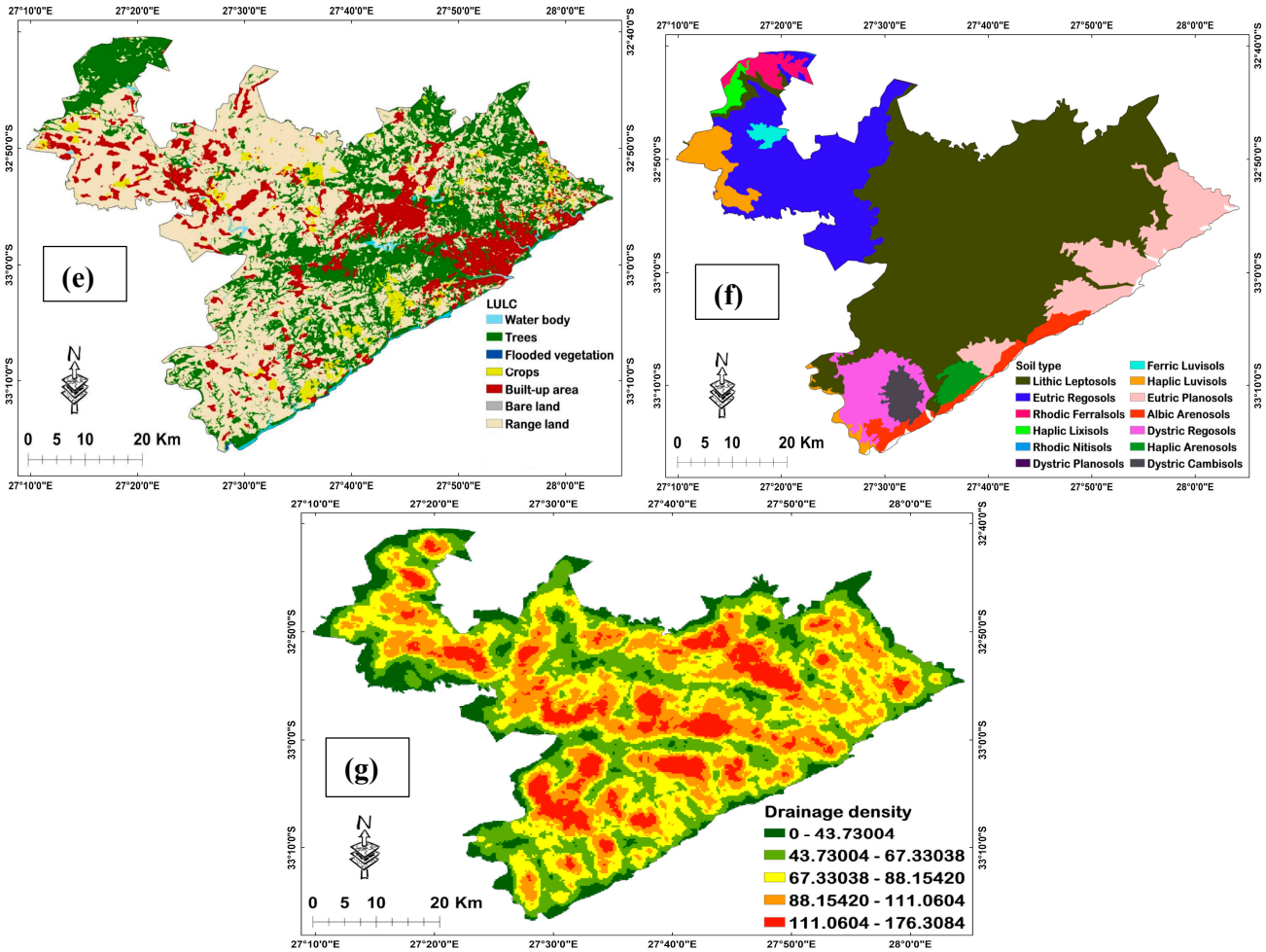

Figure 4. (**a**) Geology map of the study area; (**b**) Rainfall map; (**c**) Lineament density map; (**d**) Slope map; (**e**) LULC map; (**f**) Soil type map; (**g**) Drainage density map.

3.1.4. Slope

The study area's slope map was classified into five subclasses viz., <1.8° (flat), 1.9–2.6° (gentle), 2.7–3.4° (moderate), 3.5–4.2°, and 4.3–5° (steep) (Figure 4d). A steeper slope will result in a lesser infiltration rate because of greater runoff potential. Therefore, the highest rank (5) was assigned to the lowest slope gradient (<1.8°), which covers about 91% of the study area (Table 2), and the lowest rank (1) was assigned to the highest slope gradient (0.002% of the surface area) which is found in the north-western, central, and eastern parts.

3.1.5. LULC

The different LULC types observed in the study area are water bodies, trees, flooded vegetation, crops, built-up areas, bare land, and rangeland (Figure 4e). The result of the LULC mapping indicates that the rangeland (125 km^2) has the highest land coverage. This is followed by the trees (78 km^2), the built-up (38 km^2), the crops (9 km^2), the water bodies (2 km^2), and the bare land (1 km^2), while flooded vegetation has the least coverage (0.1 km^2). The accuracy of the LULC map was validated with the aid of Google Earth features. The Briddle Drift Dam, Nahoon River Dam, and Rooikrandsdam were all clearly marked out in the same manner as they were in Google Earth. Also, the built-up areas displayed on the LULC map show similar sectoral demarcation as observed in Google Earth. The highest rank (5) was assigned to areas covered with water bodies and flooded vegetation. In contrast, the lowest rank (1) was given to built-up areas and rangeland (Table 2).

Table 2. The assigned rank of each factor and their subclasses.

Factor	Sub-Class	Rank	Factor	Sub-Class	Rank
Geology	Quaternary sediment	5	Soil Type	Albic Arenosols	3
	Nanaga	4		Haplic Arenosols	3
	Igoda	5		Dystric Cambisols	5
	Karoo dolerite	3		Rhodic Ferralsols	3
	Tarkastad	5		Lithic Leptosols	2
	Adelaide	5		Ferric Luvisols	4
Rainfall (mm)	692–714	4		Haplic Luvisols	4
	715–735	4		Haplic Lixisols	5
	736–757	4		Rhodic Nitisols	3
	758–778	5		Dystric Planosols	2
	779–850	5		Eutric Planosols	2
Lineament Density	0–0.0002698	1		Dystric Regosols	3
	0.0002699–0.000549	2		Eutric Regosols	3
	0.0005488–0.000873	3	Drainage Density	0–43.73004	5
	0.0008726–0.001304	4		43.73005–67.33038	4
	0.0013050–0.002294	5		67.33039–88.15420	3
Slope (°)	<1.8	5		88.15421–111.0604	2
	1.9–2.6	4		111.0605–176.3084	1
	2.7–3.4	3			
	3.5–4.2	2			
	4.3–5.0	1			
LULC	Water body	5			
	Trees	3			
	Flooded vegetation	5			
	Crops	3			
	Built-up area	1			
	Bare land	2			
	Rangeland	1			

3.1.6. Soil Type

The study area comprises major soil types like Lithic Leptosols, which cover (51.43%), Eutric Regosols (30.48%), Haplic Luvisols (3.81%), Eutric Planosols (3.42%), Haplic Lixisols (2.24%), Rhodic Ferralsols (1.89%), Dystric Planosols (1.75%), Dystric Regosols (1.68%), Albic Arenosols (1.31%). Other soil types like Haplic Arenosols, Dystric Cambisols, Ferric Luvisols, and Rhodic Nitisols cover less than 1% of the area (Figure 4f). The soil types were ranked based on their water infiltration capacity (Table 2). Table 3 shows the description of different types of soil in the area.

Table 3. Description of soil types in the study area.

Soil Types	Description
Arenosols (Albic and Haplic)	Sandy loam soils with very weak or no soil development.
Luvisols (Ferric and Haplic)	Brown/reddish brown with clay to silty clay texture, moderately well to well-drained weathered soils.
Regosols (Eutric and Dystric)	Sandy loam to loam, excessively drained soils with no or little soil development.
Nitisols (Rhodic)	Dark red or dusty red clayey soils having a pronounced shiny, nut-shaped structure, silty clay to clay well-drained soil.
Lixisols (Haplic)	Red-yellow soils with subsurface accumulation of low activity clays and high base saturation, low activity clays, and a moderate to high base saturation level.
Leptosols (Lithic)	Clay loam to clay, very shallow soils over a hard rock or in unconsolidated very gravelly material, soil with no or little soil developments.
Cambisols (Dystric)	Silty clay moderately to deep and well-drained soils, weakly to moderately developed soils.
Planosols (Eutric and Dystric)	Wet soils with a light-colored, temporarily water-saturated topsoil on a low permeable subsoil, soil with low structure stability.
Ferralsols (Rhodic)	Deep, strongly weathered, yellow or red soils with a physically stable but chemically poor subsoil, clay assemblage dominated by a low activity of clays.

3.1.7. Drainage Density

The drainage density map of the study area was classified into the following five subclasses: very low (0–43.73004 km/km^2), low (43.73005–67.33038 km/km^2), moderate (67.33039–88.15420 km/km^2), high (88.15421–111.0604 km/km^2), and very high (111.0605–176.3084 km/km^2), occupying approximately 6%, 32%, 44%, 13%, and 5% of the total surface area, respectively (Figure 4g). High rank (5) was given to low drainage density, and low rank (1) was allocated to high drainage density regarding groundwater potentiality (Table 2). However, a very high drainage density subclass dominates the study area's southern, north-western, and central parts.

3.2. Results of the Models

3.2.1. Assessment of Potential Groundwater Recharge Zones Using AHP Model

The resulting GWPZ map produced using the AHP model is presented in Figure 5, and it was classified using [70] natural breaks classification technique into five subclasses: very low, low, moderate, high, and very high. The zones with high groundwater potential dominate the eastern and north-western parts of the study area, while the very poor groundwater potential zone dominates the central and northwest regions. The CR value obtained in this study is 4.5%, indicating that a fair level of consistency was used to determine the weight of the criteria.

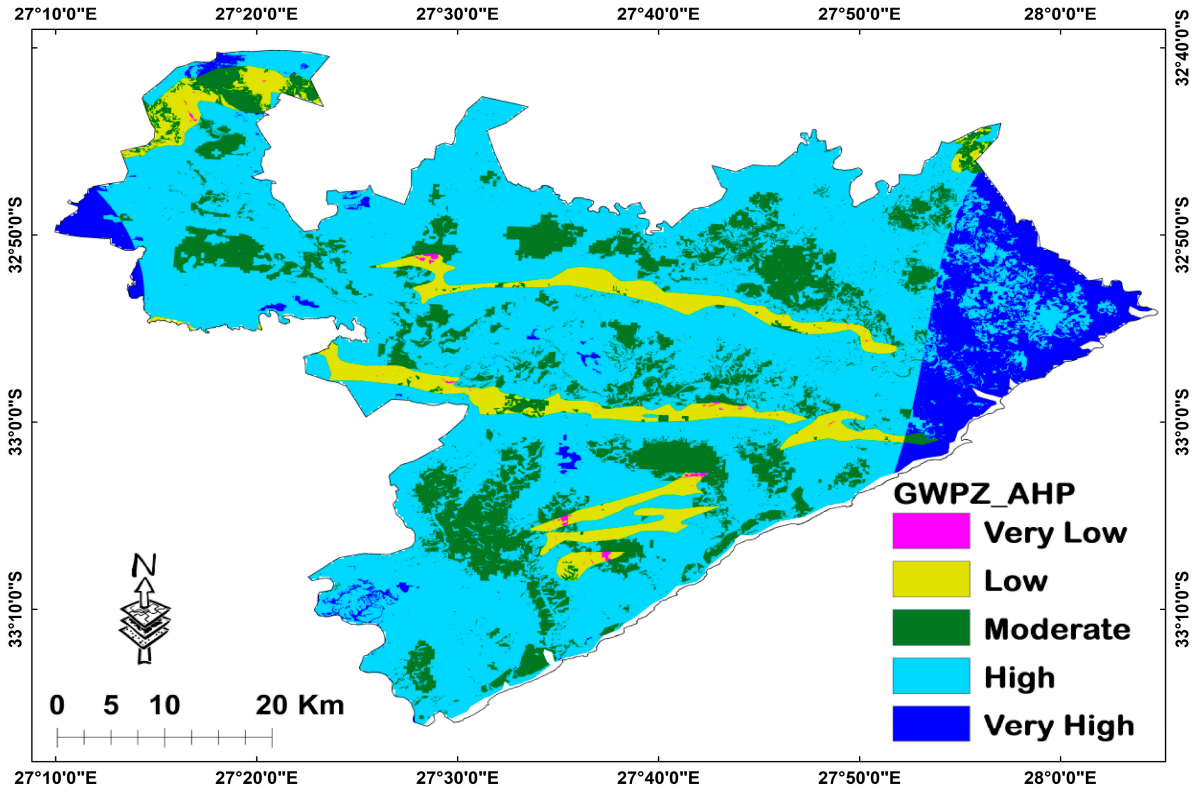

Figure 5. Groundwater potential map of the research area using analytical hierarchy process model.

3.2.2. Assessment of Potential Groundwater Recharge Zones Using FR Model

The results of the spatial correlations between the borehole and each influencing factor using the FR model are displayed in Table 4. The FR value of one indicates an average geographical correlation between the groundwater borehole's location and its conditioning factor. A value less than one denotes a low correlation, whereas a value greater than one indicates a stronger correlation [71].

Table 4. The relationship between the boreholes and factors with the FR value for each subclass.

Factor	Subclasses	No of Pixel	% of Subclass	No of BH	% of BH	FR
Geology	Adelaide	2,288,646	81.42	27	58.70	0.72
	Karoo dolerite	263,570	9.38	5	10.87	1.16
	Tarkastad	196,420	6.99	6	13.04	1.87
	Quaternary sediment	26,105	0.93	7	15.22	16.38
	Igoda	367	0.01	0	0	0.00
	Nanaga	35,689	1.27	1	2.17	1.71
Rainfall (mm)	692–714	1,373,343	48.50	8	17.39	0.36
	715–735	1,151,170	40.65	23	50.00	1.23
	736–757	202,583	7.15	9	19.57	2.73
	758–778	76,136	2.69	6	13.04	4.85
	779–850	28,436	1.00	0	0	0.00
Lineament Density	0–0.0002698	1,541,250	54.41	29	63.04	1.16
	0.0002699–0.0005487	882,092	31.13	11	23.91	0.77
	0.0005488–0.0008725	291,509	10.29	6	13.04	1.27
	0.0008726–0.001304	98,378	3.47	0	0	0.00
	0.001305–0.002294	19,947	0.70	0	0	0.00
Slope (°)	< 1.8	2,613,290	91.075	46	100	1.10
	1.9–2.6	238,781	8.322	0	0	0.00
	2.7–3.4	15,731	0.548	0	0	0.00
	3.5–4.2	1495	0.052	0	0	0.00
	4.3–5.0	72	0.003	0	0	0.00
LULC	Water body	25,859	0.914	0	0	0.00
	Trees	869,814	30.709	12	26.09	0.85
	Flooded vegetation	1095	0.039	0	0	0.00
	Crops	104,942	3.707	4	8.70	2.35
	Built-up area	419,299	14.800	19	41.30	2.79
	Bare land	9455	0.333	0	0	0.00
	Rangeland	1,402,679	49.498	11	23.91	0.48
Soil Type	Albic Arenosols	72,443	2.570	7	15.22	5.92
	Haplic Arenosols	36,374	1.290	4	8.70	6.74
	Dystric Cambisols	46,054	1.634	0	0	0.00
	Rhodic Ferralsols	42,890	1.522	0	0	0.00
	Lithic Leptosols	1,626,650	57.708	13	28.00	0.49
	Ferric Luvisols	16,996	0.603	0	0	0.00
	Haplic Luvisols	85,552	3.035	0	0	0.00
	Haplic Lixisols	18,028	0.640	0	0	0.00
	Rhodic Nitisols	281	0.010	0	0	0.00
	Dystric Planosols	730	0.026	0	0	0.00
	Eutric Planosols	283,950	10.074	15	32.61	3.24
	Dystric Regosols	119,424	4.237	2	4.35	1.03
	Eutric Regosols	469,401	16.653	5	10.87	0.65
Drainage Density	0–43.73004	308,136	10.953	4	8.70	0.79
	43.73005–67.33038	727,521	25.860	18	39.13	1.51
	67.33039–88.1542	825,658	29.348	16	34.78	1.19
	88.15421–111.0604	645,179	22.933	4	8.70	0.38
	111.0605–176.3084	306,797	10.905	4	8.70	0.80

The FR results show that the Quaternary sediments subclass of the geology has the highest value of FR (16.38), followed by Tarkastad (1.78), Nanaga (1.71), Karoo dolerite (1.16), Adelaide (0.72), and Igoda, which has FR value of zero. Also, the highest FR value (4.85) for rainfall subclasses was found in regions receiving precipitation between 758–778 mm, followed by 736–757 mm (2.73), 715–735 mm (1.23), and 692–714 mm (0.36). The region with a lot of precipitation (779–850 mm) is the lowest (FR = 0) and has no potential. The subclass of lineament density with the highest groundwater potentiality is 0.0005488–0.0008725 km/km^2 (FR = 1.27), followed by 0–0.0002698 km/km^2 (FR = 1.16) and

0.0002699–0.0005487 km/km^2 (FR = 0.77). The lineament subclass 0.0008726–0.001304 km/km^2 and 0.001305–0.002294 km/km^2 have the lowest FR value of zero.

The highest value of FR (1.10) was seen in a slope degree class of <1.8°. The FR is zero for slope subclasses 1.9–2.6°, 2.7–3.4°, 3.5–4.2°, and 4.3–5.0°. Among the LULC subclasses, the built-up area has the highest FR value of 2.79, followed by the crops subclass (FR = 2.35). The tree and the range land subclasses have FR values of 0.85 and 0.48, respectively. The water body and bare land have an FR value of zero. The highest value of FR (6.74) for soil type subclasses was observed in the area occupied by Haplic Arenosols, followed by Albic Arenosols (FR = 5.92), Eutric Planosols (FR = 3.24), Dystric Regosols (FR = 1.03), Eutric Regosols (FR = 0.65), and Lithic Leptosols (FR = 0.49). The Dystric Cambisols, Ferralsols Rhodic, Ferric Luvisols, Haplic Luvisols, Haplic Lixisols, Rhodic Nitisols, and Dystric Planosols subclasses have an FR value of zero. Lastly, high groundwater potentiality occurs mainly in the drainage density ranges of 43.73005–67.33038 km/km^2 (FR = 1.51), 67.33039–88.1542 km/km^2 (FR = 1.19), 111.0605–176.3084 km/km^2, 0–43.73004 km/km^2 (FR = 0.79), and 88.15421–111.0604 km/km^2 (FR = 0.38).

The integrated GWPZ map was classified into five classes, varying from very low to very high groundwater potentiality (Figure 6).

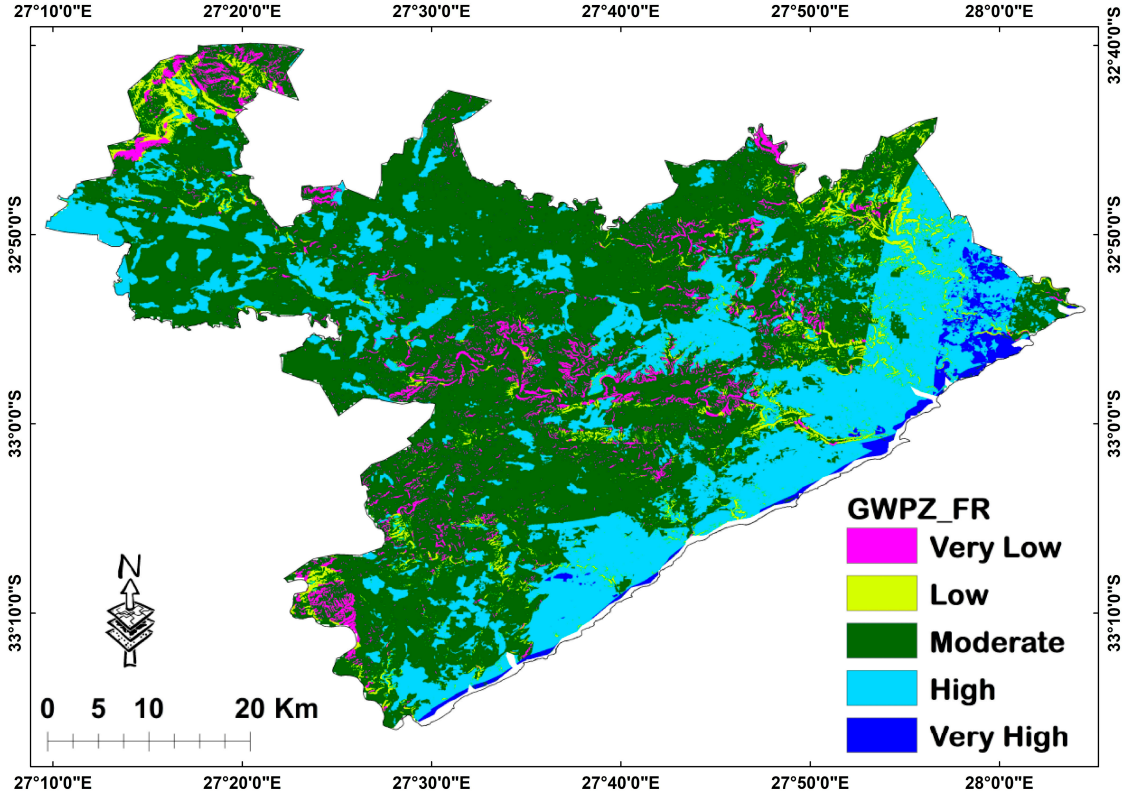

Figure 6. Groundwater potential map of the research area using frequency ratio model.

4. Discussion

4.1. Delineation of Potential Groundwater Recharge Zones (GWPZ) Using AHP Model

All groundwater controlling factors were integrated: rainfall, geology, slope, drainage density, LULC, lineament density, and soil. The delineation of the GWPZ map using the AHP model was carried out based on the weighted overlay technique according to Equation (3) [15,35,36].

The pairwise comparison results revealed that rainfall is the most significant factor that contributes to the groundwater occurrence in the study area, accounting for about 38.18%, followed by the geology (25.01%), slope (12.11%), and drainage density (9.09%). The LULC and soil factors are the least influential at 5.43% and 3.94%, respectively. The pairwise comparison results align with [72], who reported that rainfall, geology, and slope are the

main controlling factors of groundwater potential since groundwater recharge in the area relies greatly on rainfall. Meanwhile, according to [73], the recharge link to rainfall is the key factor influencing the aquifers in this present study area. Therefore, the rainfall factor has the highest weight. The AHP map shows that the moderate to very high potentiality for groundwater in the area is present in the area covered with the sedimentary rocks of the Adelaide and Tarkastad Supergroup (sandstones and mudstones), Quaternary sediments (claystone and coastal sands), Nanaga Formation (calcareous sandstones), and Igoda Formation (limestones), having high hydraulic conductivity, porosity, and permeability [74]. Also, areas with high amounts of rainfall coupled with high infiltration capacity due to flat slopes, moderate to high lineament density, and appropriation of Lithic Leptosols, Haplic Luvisols, Albic Arenosols, and Eutric Planosols show moderate to very high groundwater potentiality [75–77]. However, very high areas for groundwater potentiality found in the eastern, central, and western parts are relatively small.

Similar to existing literature [13,78,79], areas with low rainfall, steep slope, soil with little or no development, low lineament density, and high drainage density found in the south-central and north-western parts of the study area show very poor and poor groundwater potentiality. This finding indicates that rainfall and slope factors significantly control groundwater development in the semi-arid region. Also, the lineament density helps the groundwater system's infiltration ability [80]. Contrary to the findings of [27], who noted that very high groundwater potential zones fall in the high drainage density subclass, in this present study, the high drainage density subclass has very poor groundwater potential due to the occurrence of an impervious layer of Karoo dolerite beneath it. Furthermore, due to their low hydraulic conductivity, these Karoo dolerites are associated with very poor and poor potential areas [81]. The hydraulic conductivity is an important aquifer characteristic that governs a lithology's groundwater storage and recharge potential [74]. However, the Karoo dolerites (sills and dykes) created fractures or cracks in the Karoo basin, which allow groundwater flow, thus increasing groundwater potentiality in its vicinity [82]. The AHP model result computed that about 8.90% of the total area falls under very high groundwater potentiality, while 65.57% under high potentiality, which covers the largest part of the study area (Table 5). The moderate potential zone covers about 17.60%, the low potential zone covers around 7.87%, and the very poor potential zone constitutes around 0.13%.

Table 5. The distribution of groundwater potential classes based on the AHP and FR models.

	AHP Model			FR Model		
	Range	**Area (km^2)**	**Area (%)**	**Range**	**Area (km^2)**	**Area (%)**
Very Low	257.46–301.50	32.33	0.13	23.35–81.23	1012.76	4.04
Low	301.50–345.54	1954.31	7.80	81.23–215.51	1218.18	4.86
Moderate	345.54–389.59	4412.02	17.60	215.51–366.00	15,610.86	62.28
High	389.59–433.63	16,437.17	65.57	366.00–442.40	6787.63	27.08
Very High	433.63–477.67	2230.52	8.90	442.40–613.73	436.91	1.74

4.2. Delineation of Potential Groundwater Potential Zones Using FR Model

The resultant FR model map reveals that 4.04%, 4.86%, 62.28%, 27.08%, and 1.74% areas under very low, low, moderate, high, and very high groundwater potential zones, respectively. The analysis of FR for the relationship between groundwater borehole and geology percent shows that geology factor subclass Quaternary sediment has the highest FR value of 16.38 among all factor's subclasses, showing a stronger correlation with groundwater potentiality [71]. This finding corroborates the result of [83], who reported that Quaternary sediment plays a vital role in groundwater storage by providing maximum groundwater-yielding capacity for sustainable groundwater supply. This subclass constitutes about 15% of the boreholes in the study area. The Nanaga Formation (FR = 1.71), Tarkastad (FR = 1.87), and Adelaide (FR = 0.72) Subgroups are composed of sedimentary rocks (mudstones and sandstones) which have been intruded by Karoo dolerites, resulting

in secondary porosity in the form of fractures and weathering, allowing groundwater occurrence [84]. These subclasses account for about 2.17%, 13.04%, and 58.70% of the boreholes available in the study area; thus, the abovementioned geology subclasses have a reasonable probability for groundwater occurrence [39]. Karoo dolerite, a groundwater localizer in the Karoo basin [82], attained an FR value of 1.16. Lastly, the Igoda Formation has an FR value of 0 due to its occurrence limitation (0.01% of the surface area).

The assessment of rainfall indicated that subclasses of 758–778 mm have the highest value of FR (4.85), with 13.04% of boreholes in the area. Meanwhile, the region with the highest rainfall (779–850 mm) has an FR value of 0 due to its limitation in terms of area covered (1%), with the presence of zero borehole in that class, since the FR model uses the probabilistic relationship between boreholes and the factor's subclasses [13]. Similarly, the assessment of lineament density shows that density subclasses of 0.0008726–0.001304 km/km^2 (high) and 0.001305–0.002294 km/km^2 (very high) have an FR value of 0. These subclasses cover a total surface area of 3.47% and 0.70%, respectively. The density subclass 0.0005488–0.0008725 km/km^2 (moderate) has the highest value of FR (1.27), with 13.04% of boreholes in the subclass. Therefore, it reflects better groundwater potential than other lineament density subclasses. In the case of the slope, the gentle slope (<1.8°) subclass indicates the highest FR (0.10) in the slope factor. This subclass comprises 100% of the boreholes in the area, while the FR values for the other four subclasses are all 0. FR values decrease by increasing subclasses of slope gradient. Similar FR ratio trends for slope factors were also observed in the literature [13,39,85].

In terms of LULC, it can be observed that the built-up area, crops, trees, and rangeland subclasses have FR values of 2.79, 2.35, 0.85, and 0.48, respectively, signifying that the likelihood of groundwater occurrence in these LULC subclasses is very high. Contrary to existing literature [5,39,86], the built-up in the LULC factor has the highest FR value than the remaining subclasses. The boreholes in the study area are primarily located in built-up areas with significant water demand, and they are used as an alternate source of water resources for residents. Therefore, it was assumed that built-up areas would have a high FR value. This finding agrees with the report of [13] concerning the connection between boreholes and the subclasses of LULC.

Regarding the spatial relationships between the boreholes and soil type factor, the Haplic Arenosols subclass attained the highest value of FR (6.74), followed by the Albic Arenosols subclass (5.92), indicating a strong relationship with groundwater potentiality. Arenosols soil types are mostly well-developed soils with a high percentage of large pores, contributing to their rapid drainage and low water storage capacity [87]. The highest frequency ratio values (FR = 1.51 and 1.19, respectively) were found at the places with drainage densities of 43.73005–67.33038 and 67.33039–88.1542 km/km^2, displaying a positive correlation with groundwater potentiality.

4.3. Model Validation

The result of models must be validated to check the proficiency of the predicted results in accurately mapping groundwater potential zones [40]. The ROC curve was generated by correlating the existing groundwater borehole locations with the groundwater potential map using the testing datasets [88]. The ROC curves of the resultant GWPZ maps using the AHP and FR models are displayed in Figure 7a,b. The graphs revealed that the FR model (AUC = 85.3%) performed better than the AHP model (AUC = 83.2%). The AUC values, in terms of prediction accuracy, were classified into poor (<50%), average (50–70%), good (70–80%), very good (80–90%), and excellent (90–100%), according to [89]. Based on these classifications, this study's AHP and FR models showed very good accuracy in groundwater potential assessment.

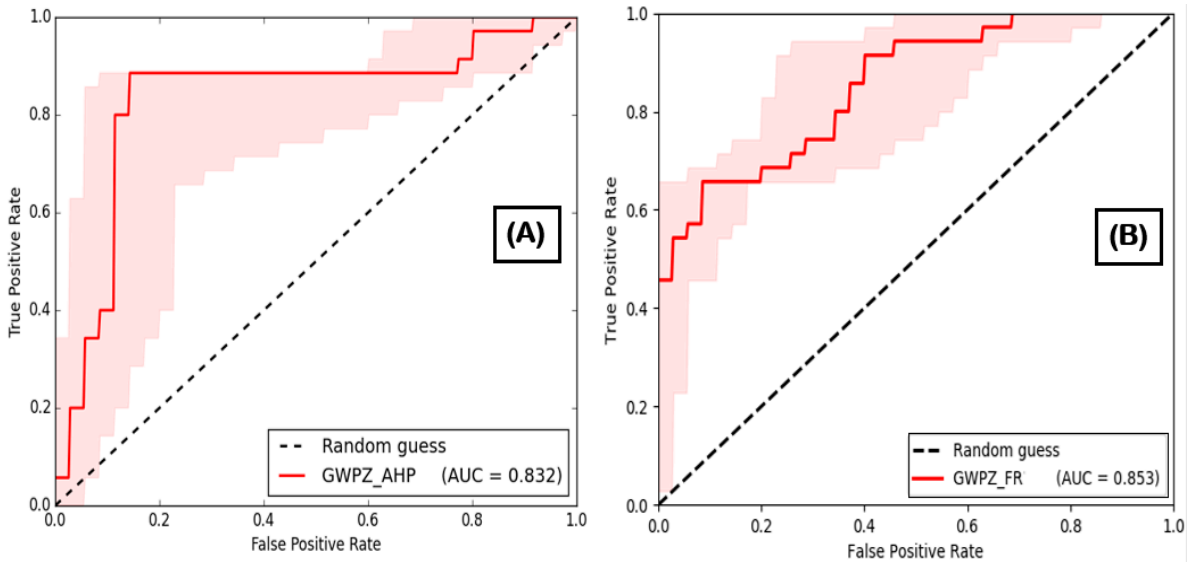

Figure 7. The ROC curves for the validation dataset: (**A**) AHP and (**B**) FR model.

5. Conclusions

Delineation of groundwater potential zones in BCMM in the Eastern Cape Province of South Africa was assessed through AHP and FR models. This research combined conventional datasets and satellite images to generate maps of seven factors (geology, rainfall, soil type, slope, drainage density, lineament density, and LULC), that control groundwater occurrence. These resultant groundwater potential maps were validated to confirm the accuracy of the AHP and FR models in mapping groundwater potential zones.

Thirty-four (34) boreholes were used to validate each model using the AUC analysis. The AUC for the AHP model is 83.2% and 85.3% for the FR model. Therefore, the groundwater potential mapped by the FR is more accurate and reliable than the AHP model. The weights and rankings given to each class and subclass directly impact the accuracy of the AHP model for groundwater potential delineation. Hence, in-depth research and knowledge of groundwater occurrence factors are needed. The FR determines a ratio of factors that yields more accurate results, whereas the model does not require more user knowledge to set ranks or weights. The government or other non-government entities can choose the locations with good groundwater potential in the resultant maps for groundwater exploration projects. This research presents a straightforward and systematic approach to identifying groundwater potential zones using forefront geospatial techniques. However, this method can locate several groundwater recharge zones in other regions, thereby contributing to rational exploitation and ensuring the sustainable development of groundwater resources. It is recommended that the findings should be followed with further quantitative assessments of groundwater recharge and other relevant research to achieve more detailed groundwater potential mapping. Finally, the findings of this study will assist policy makers and non-governmental organizations in developing sustainable management plans for groundwater resources.

Author Contributions: Conceptualization, G.O.A.; methodology, G.O.A. and K.H.T.; software, K.H.T. and B.K.P.; validation, G.O.A., K.H.T., B.K.P. and O.G.; formal analysis, G.O.A. and K.H.T.; investigation, G.O.A.; resources, K.H.T. and B.K.P.; data curation, G.O.A.; writing—original draft preparation, G.O.A.; writing—review and editing, K.H.T., B.K.P. and O.G.; visualization, G.O.A.; supervision, O.G. and B.P; project administration, G.O.A. and K.H.T.; funding acquisition, O.G. and B.K.P. All authors have read and agreed to the published version of the manuscript.

Funding: This research received no external funding.

Data Availability Statement: Not applicable.

Acknowledgments: The authors thank Gbenga Abayomi Afuye (University of Fort Hare) and Babawande Emmanuel Olawale (University of Fort Hare) for their support. Also, we wish to acknowledge the Buffalo City Metropolitan Municipality for providing the borehole data and granting access permits to the borehole sites.

Conflicts of Interest: The authors declare no conflict of interest.

References

1. Arabameri, A.; Rezaei, K.; Cerda, A.; Lombardo, L.; Rodrigo-Comino, J. GIS-based groundwater potential mapping in Shahroud plain, Iran. A comparison among statistical (bivariate and multivariate), data mining and MCDM approaches. *Sci. Total Environ.* **2019**, *658*, 160–177. [CrossRef]
2. Mogaji, K.A.; Omobude, O.B. Modeling of geoelectric parameters for assessing groundwater potentiality in a multifaceted geologic terrain, Ipinsa Southwest, Nigeria-A GIS-based GODT approach. *NRIAG J. Astron. Geophys.* **2017**, *6*, 434–451. [CrossRef]
3. Chen, W.; Li, H.; Hou, E.; Wang, S.; Wang, G.; Panahi, M.; Li, T.; Peng, T.; Guo, C.; Niu, C.; et al. GIS-based groundwater potential analysis using novel ensemble weights-of-evidence with logistic regression and functional tree models. *Sci. Total Environ.* **2018**, *634*, 853–867. [CrossRef]
4. Pradhan, R.M.; Guru, B.; Pradhan, B.; Biswal, T.K. Integrated multi-criteria analysis for groundwater potential mapping in Precambrian hard rock terranes (North Gujarat), India. *Hydrol. Sci. J.* **2021**, *6*, 961–978. [CrossRef]
5. Das, S. Comparison among influencing factor, frequency ratio, and analytical hierarchy process techniques for groundwater potential zonation in Vaitarna basin, Maharashtra, India. *Groundw. Sustain. Dev.* **2019**, *8*, 617–629. [CrossRef]
6. Taheri, K.; Taheri, M.; Parise, M. Impact of intensive groundwater exploitation on an unprotected covered arst aquifer: A case study in Kermanshah Province, western Iran. *Environ. Earth Sci.* **2016**, *75*, 1221. [CrossRef]
7. Majidipour, F.; Najafi, S.M.B.; Taheri, K.; Fathollahi, J.; Missimer, T.M. Index-based groundwater sustainability assessment in the socio-economic context: A case study in the Western Iran. *Environ. Manag.* **2021**, *67*, 648–666. [CrossRef]
8. Taheri, K.; Missimer, T.M.; Amini, V.; Bahrami, J.; Omidipour, R. A GIS-expert-based approach for groundwater quality monitoring network design in an alluvial aquifer: A case study and a practical guide. *Environ. Monit. Assess.* **2020**, *192*, 1–20. [CrossRef]
9. Owolabi, S.T.; Madi, K.; Kalumba, A.M. Comparative evaluation of spatio-temporal attributes of precipitation and streamflow in Buffalo and Tyume Catchments, Eastern Cape, South Africa. *Environ. Dev. Sustain.* **2021**, *23*, 4236–4251. [CrossRef]
10. Baudoin, M.A.; Vogel, C.; Nortje, K.; Naik, M. Living with drought in South Africa: Lessons learnt from the recent El Niño drought period. *Int. J. Disaster Risk Reduct.* **2017**, *23*, 128–137. [CrossRef]
11. Nolte, A.; Eley, M.; Schöniger, M.; Gwapedza, D.; Tanner, J.; Mantel, S.K.; Scheihing, K. Hydrological modelling for assessing spatio-temporal groundwater recharge variations in the water-stressed Amathole Water Supply System, Eastern Cape, South Africa: Spatially distributed groundwater recharge from hydrological model. *Hydrol. Process.* **2021**, *35*, 14264. [CrossRef]
12. Mahlalela, P.T.; Blamey, R.C.; Hart, N.C.G.; Reason, C.J.C. Drought in the Eastern Cape region of South Africa and trends in rainfall characteristics. *Clim. Dyn.* **2020**, *55*, 2743–2759. [CrossRef]
13. Muavhi, N.; Thamaga, K.H.; Mutoti, M.I. Mapping groundwater potential zones using relative frequency ratio, analytic hierarchy process and their hybrid models: Case of Nzhelele-Makhado area in South Africa. *Geocarto Int.* **2022**, *37*, 6311–6330. [CrossRef]
14. Das, S.; Gupta, A.; Ghosh, S. Exploring groundwater potential zones using MIF technique in semi-arid region: A case study of Hingoli district, Maharashtra. *Spat. Inf. Res.* **2017**, *25*, 749–756. [CrossRef]
15. Arulbalaji, P.; Padmalal, D.; Sreelash, K. GIS and AHP techniques based delineation of groundwater potential zones: A case study from Southern Western Ghats. *India Sci. Rep.* **2019**, *9*, 2082. [CrossRef]
16. Adesola, G.O.; Gwavava, O.; Liu, K. Hydrological Evaluation of the Groundwater Potential in the Fractured Karoo Aquifer Using Magnetic and Electrical Resistivity Methods: Case Study of the Balfour Formation, Alice, South Africa. *Int. J. Geophys.* **2023**, *2023*, 1891759. [CrossRef]
17. Hasan, M.; Shang, Y.; Akhter, G.; Khan, M. Geophysical investigation of fresh-saline water interface: A case study from South Punjab, Pakistan. *Groundwater* **2017**, *55*, 841–856. [CrossRef]
18. Olatinsu, O.B.; Salawudeen, S.Y. Integrated geophysical investigation of groundwater potential and bedrock structure in Precambrian basement rocks of Ife, southwest Nigeria. *Groundw. Sustain. Dev.* **2021**, *14*, 100616. [CrossRef]
19. McLachlan, P.; Blanchy, G.; Chambers, J.; Sorensen, J.; Uhlemann, S.; Wilkinson, P.; Binley, A. The application of electromagnetic induction methods to reveal the hydrogeological structure of a riparian wetland. *Water Resour. Res.* **2021**, *57*, e2020WR029221. [CrossRef]
20. Pradhan, R.M.; Deshmukh, R.; Chandrasekhar, E.; Balamurugan, G.; Biswal, T.K. Geoelectrical studies for groundwater exploration in fractured rock terrane (Ambaji basin, India). In Proceedings of the Conference of the Arabian Journal of Geosciences, Sousse, Tunisia, 25–28 November 2019; pp. 511–514. [CrossRef]
21. Sharma, S.P.; Baranwal, V.C. Delineation of groundwater-bearing fracture zones in a hard rock area integrating very low frequency electromagnetic and resistivity data. *J. Appl. Geophys.* **2005**, *2*, 155–166. [CrossRef]
22. Raji, W.O.; Abdulkadir, K.A. Evaluation of groundwater potential of bedrock aquifers in geological sheet 223 Ilorin, Nigeria, using geo-electric sounding. *Appl. Water Sci.* **2020**, *10*, 220. [CrossRef]

23. Akingboye, A.S.; Bery, A.A.; Kayode, J.S.; Ogunyele, A.C.; Adeola, A.O.; Omojola, O.O.; Adesida, A.S. Groundwater-yielding capacity, water-rock interaction, and vulnerability assessment of typical gneissic hydrogeologic units using geoelectrohydraulic method. *Acta Geophys.* **2023**, *71*, 697–721. [CrossRef]
24. Pradhan, R.M.; Singh, A.; Ojha, A.K.; Biswal, T.K. Structural controls on bedrock weathering in crystalline basement terranes and its implications on groundwater resources. *Sci. Rep.* **2022**, *1*, 11815. [CrossRef] [PubMed]
25. Akingboye, A.S.; Bery, A.A.; Kayode, J.S.; Asulewon, A.M.; Bello, R.; Agbasi, O.E. Near-surface crustal architecture and geohydrodynamics of the crystalline basement terrain of Araromi, Akungba-Akoko, SW Nigeria, derived from multi-geophysical methods. *Nat. Resour. Res.* **2022**, *31*, 215–236. [CrossRef]
26. Nampak, H.; Pradhan, B.; Manap, M.A. Application of GIS based data driven evidential belief function model to predict groundwater potential zonation. *J. Hydrol.* **2014**, *513*, 283–300. [CrossRef]
27. Guru, B.; Seshan, K.; Bera, S. Frequency ratio model for groundwater potential mapping and its sustainable management in cold desert, India. *J. King Saud. Univ.-Sci.* **2017**, *29*, 333–347. [CrossRef]
28. Kumar, V.A.; Mondal, N.C.; Ahmed, S. Identification of groundwater potential zones using RS, GIS and AHP techniques: A case study in a part of Deccan Volcanic Province (DVP), Maharashtra, India. *J. Indian. Soc. Remote Sens.* **2020**, *48*, 497–511. [CrossRef]
29. Singh, L.K.; Jha, M.K.; Chowdary, V.M. Assessing the accuracy of GIS-based Multi-Criteria Decision Analysis approaches for mapping groundwater potential. *Ecol. Indicat.* **2018**, *91*, 24–37. [CrossRef]
30. Rahmati, O.; Pourghasemi, H.R.; Melesse, A.M. Application of GIS-based data driven random forest and maximum entropy models for groundwater potential mapping: A case study at Mehran Region, Iran. *Catena* **2016**, *137*, 360–372. [CrossRef]
31. Kim, J.C.; Jung, H.S.; Lee, S. Groundwater productivity potential mapping using frequency ratio and evidential belief function and artificial neural network models: Focus on topographic factors. *J. Hydroinformatics* **2018**, *20*, 1436–1451. [CrossRef]
32. Andualem, T.G.; Demeke, G.G. Groundwater potential assessment using GIS and remote sensing: A case study of Guna tana landscape, upper Blue Nile Basin, Ethiopia. *J. Hydrol. Reg. Stud.* **2019**, *24*, 100610–100613. [CrossRef]
33. Ahirwar, S.; Malik, M.S.; Ahirwar, R.; Shukla, J.P. Identification of suitable sites and structures for artificial groundwater recharge for sustainable groundwater resource development and management. Groundwater Sustain. *Develop* **2020**, *11*, 100388. [CrossRef]
34. Jenifer, M.A.; Jha, M.K. Comparison of analytical hierarchy process, catastrophe and entropy techniques for evaluating groundwater prospect of hard-rock aquifer systems. *J. Hydrol.* **2017**, *548*, 605–624. [CrossRef]
35. Kumar, A.; Krishna, A.P. Assessment off groundwater potential zones in coal mining impacted hard-rock terrain of India by integrating geospatial and analytic hierarchy process (AHP) approach. *Geocarto Int.* **2018**, *33*, 105–129. [CrossRef]
36. Saranya, T.; Saravanan, S. Groundwater potential zone mapping using analytical hierarchy process (AHP) and GIS for Kancheepuram District, Tamilnadu, India. *Model. Earth Syst. Environ.* **2020**, *6*, 1105–1122. [CrossRef]
37. Taheri, K.; Missimer, T.M.; Taheri, M.; Moayedi, H.; Mohseni Pour, F. Critical zone assessments of an alluvial aquifer system using the multi-influencing factor (MIF) and analytical hierarchy process (AHP) models in Western Iran. *Nat. Resour. Res.* **2020**, *29*, 1163–1191. [CrossRef]
38. Chowdary, V.; Chakraborthy, D.; Jeyaram, A.; Murthy, Y.K.; Sharma, J.; Dadhwal, V. Multi-Criteria decision making approach for watershed prioritization using analytic hierarchy process technique and GIS. *Water Resour. Manag.* **2013**, *27*, 3555–3571. [CrossRef]
39. Moghaddam, D.D.; Rezaei, M.; Pourghasemi, H.R.; Pourtaghie, Z.S.; Pradhan, B. Groundwater spring potential mapping using bivariate statistical model and GIS in the Taleghan watershed, Iran. *Arab. J. Geosci.* **2015**, *8*, 913–929. [CrossRef]
40. Das, S.; Pardeshi, S.D. Integration of different influencing factors in GIS to delineate groundwater potential areas using IF and FR techniques: A study of Pravara basin, Maharashtra, India. *Appl. Water Sci.* **2018**, *8*, 197. [CrossRef]
41. Trabelsi, F.; Lee, S.; Khlifi, S.; Arfaoui, A. Frequency ratio model for mapping groundwater potential zones using GIS and remote sensing; Medjerda Watershed Tunisia. In *Advances in Science, Technology & Innovation*; Springer Publishing: New York, NY, USA, 2019; pp. 341–345. [CrossRef]
42. Lee, S.; Kim, Y.S.; Oh, H.J. Application of a weights-of-evidence method and GIS to regional groundwater productivity potential mapping. *J. Environ. Manag.* **2012**, *1*, 91–105. [CrossRef]
43. Nejad, S.G.; Falah, F.; Daneshfar, M.; Haghizadeh, A.; Rahmati, O. Delineation of groundwater potential zones using remote sensing and GIS-based data-driven models. *Geocarto Int.* **2017**, *2*, 167–187.
44. Sahoo, S.; Munusamy, S.B.; Dhar, A.; Kar, A.; Ram, P. Appraising the accuracy of multiclass frequency ratio and weights of evidence method for delineation of regional groundwater potential zones in canal command system. *Water Resour. Manag.* **2017**, *14*, 4399–4413. [CrossRef]
45. Rahmati, O.; Kornejady, A.; Samadi, M.; Nobre, A.D.; Melesse, A.M. Development of an automated GIS tool for reproducing the HAND terrain model. *Environ. Model. Softw.* **2018**, *102*, 1–12. [CrossRef]
46. Antonakos, A.K.; Voudouris, K.S.; Lambrakis, N.I. Site selection for drinking-water pumping boreholes using a fuzzy spatial decision support system in the Korinthia prefecture, SE Greece. *Hydrogeol. J.* **2014**, *8*, 1763–1776. [CrossRef]
47. Rahmati, O.; Melesse, A.M. Application of Dempster–Shafer theory, spatial analysis and remote sensing for groundwater potentiality and nitrate pollution analysis in the semi-arid region of Khuzestan, Iran. *Sci. Total Environ.* **2016**, *568*, 1110–1123. [CrossRef]
48. Ozdemir, A. GIS-based groundwater spring potential mapping in the Sultan Mountains (Konya, Turkey) using frequency ratio, weights of evidence and logistic regression methods and their comparison. *J. Hydrol.* **2011**, *411*, 290–308. [CrossRef]

49. Naghibi, S.A.; Pourghasemi, H.R.; Pourtaghi, Z.S.; Rezaei, A. Groundwater qanat potential mapping using frequency ratio and Shannon's entropy models in the Moghan watershed, Iran. *Earth Sci. Inform.* **2015**, *8*, 171–186. [CrossRef]
50. Golkarian, A.; Naghibi, S.A.; Kalantar, B.; Pradhan, B. Groundwater potential mapping using C5.0, random forest, and multivariate adaptive regression spline models in GIS. *Environ. Monit. Assess.* **2018**, *3*, 149. [CrossRef]
51. Golkarian, A.; Rahmati, O. Use of a maximum entropy model to identify the key factors that influence groundwater availability on the Gonabad Plain. *Iran. Env. Earth Sci.* **2018**, *77*, 369. [CrossRef]
52. Chenini, I.; Mammou, A.B. Groundwater recharge study in arid region: An approach using GIS techniques and numerical modeling. *Comput. Geosci.* **2010**, *6*, 801–817. [CrossRef]
53. Naghibi, S.A.; Pourghasemi, H.R.; Abbaspour, K.A. comparison between ten advanced and soft computing models for groundwater qanat potential assessment in Iran using R and GIS. *Theor. Appl. Climatol.* **2018**, *131*, 967–984. [CrossRef]
54. Saaty, T.L. *The Analytic Hierarchy Process: Planning, Priority Setting, Resource Allocation*; McGraw: New York, NY, USA, 1980; p. 281.
55. Nel, J.; Colvin, C.; Le Maitre, D.; Smith, J.; Haines, I. *South Africa's Strategic Water Source Areas (No. CSIR/NRE/ECOS/ER/2013/0031/a)*; WWF-SA: Cape Town, South Africa, 2013; p. 27.
56. Department of Water and Sanitation (DWS). *Amatole Water Supply System Reconciliation Strategy: Status Report: October 2016*; Department of Water and Sanitation (DWS): Pretoria, South Africa, 2016; p. 90.
57. Dube, R.A.; Maphosa, B.; Fayemiwo, O.M. *Adaptive Climate Change Technologies and Approaches for Local Governments: Water Sector Response*; WRC Report No. TT; Water Research Commission: Pretoria, South Africa, 2016; Volume 663, p. 16.
58. Botai, C.M.; Botai, J.O.; Adeola, A.M.; de Wit, J.P.; Ncongwane, K.P.; Zwane, N.N. Drought risk analysis in the Eastern Cape Province of South Africa: The copula lens. *Water* **2020**, *12*, 1938. [CrossRef]
59. Cobbing, J. *Groundwater for Rural Water Supplies in South Africa*; Nelson Mandela Metropolitan University: Gqeberha, South Africa; SLR Consulting (Pty) Ltd.: Pretoria, South Africa, 2014.
60. Cobbing, J.E.; de Wit, M. The Grootfontein aquifer: Governance of a hydro-social system at Nash equilibrium. *South. Afr. J. Sci.* **2018**, *114*, 20170230. [CrossRef] [PubMed]
61. Olivier, D.W.; Xu, Y. Making effective use of groundwater to avoid another water supply crisis in Cape Town, South Africa. *Hydrogeol. J.* **2019**, *27*, 823–826. [CrossRef]
62. Algaydi, B.A.M.; Subyani, A.M.; Hamza, M.H.M.M. Investigation of groundwater potential zones in hard rock Terrain, Wadi Na'man, Saudi Arabia. *Groundwater* **2019**, *57*, 940–950. [CrossRef]
63. Statistic South Africa. *Census 2011: Census in Brief*; Statistics South Africa: Pretoria, South Africa, 2012.
64. Department of Water Affairs and Forestry (DWAF). *State-of-Rivers Report: Buffalo River System (River Health Programme)*; Department of Water Affairs and Forestry: KwaZulu-Natal, South Africa, 2004; Volume 8, p. 102.
65. Johnson, M.; van Vuuren, C.; Visser, J.; Cole, D.; de Wickens, H.; Christie, A.; Roberts, D. The Foreland Karoo Basin, South Africa. In *African Sedimentary Basins of the World*; Selley, R., Ed.; Elsevier: Amsterdam, The Netherlands, 1997; Volume 3, pp. 269–317.
66. Department of Water Affairs and Forestry (DWAF). *Development of a Reconciliation Strategy for the Amatole Bulk Water Supply System*; Final Report (No. PWMA 12/R00/00/2608); Department of Water Affairs and Forestry: KwaZulu-Natal, South Africa, 2008; p. 134.
67. Hashim, M.; Ahmad, S.; Johari, M.A.M.; Pour, A.B. Automatic lineament extraction in a heavily vegetated region using Landsat Enhanced Thematic Mapper (ETM+) imagery. *Adv. Space Res.* **2013**, *51*, 874–890. [CrossRef]
68. Sener, S.; Sener, E.; Karaguzel, R. Solid waste disposal site selection with GIS and AHP methodology: A case study in Senirkent-Uluborly (Isparta) Basin, Turkey. *Environ. Monit. Assess.* **2011**, *173*, 533–554. [CrossRef]
69. Pourtaghi, Z.S.; Pourghasemi, H.R. GIS-based groundwater spring potential assessment and mapping in the Birjand Township, southern Khorasan Province Iran. *Hydrogeology* **2014**, *22*, 643–662. [CrossRef]
70. Jenks, G.F. The data model concept in statistical mapping. *Int. Year Book. Cartogr.* **1967**, *7*, 186–190.
71. Oh, H.J.; Lee, S. Assessment of ground subsidence using GIS and the weights-of-evidence model. *Eng. Geol.* **2010**, *115*, 36–48. [CrossRef]
72. Jasrotia, A.S.; Kumar, R.; Saraf, A.K. Delineation of groundwater recharge sites using integrated remote sensing and GIS in Jammu district, India. *Int. J. Remote Sens.* **2007**, *28*, 5019–5036. [CrossRef]
73. Stroebel, D.H.; Thiart, C.; de Wit, M. Towards defining a baseline status of scarce groundwater resources in anticipation of hydraulic fracturing in the Eastern Cape Karoo, South Africa: Salinity, aquifer yields and groundwater levels. *Geol. Soc. Lond. Spec. Publ.* **2019**, *479*, 129–145. [CrossRef]
74. Barlow, P.M.; Leake, S.A. *Streamflow Depletion by Wells: Understanding and Managing the Effects of Groundwater Pumping on Streamflow*; US Geological Survey: Reston, VA, USA, 2012; Volume 1376, 84p. [CrossRef]
75. Xu, Y.; Lin, L.; Jia, H. *Groundwater Flow Conceptualization and Storage Determination of the Table Mountain Group (TMG) Aquifers*; WRC Report, (1419/1); Water Research Commission: Pretoria, South Africa, 2009; p. 9.
76. Kindie, A.T.; Enku, T.; Moges, M.A.; Geremew, B.S.; Atinkut, H.B. Spatial analysis of groundwater potential using GIS based multi criteria decision analysis method in Lake Tana Basin, Ethiopia. In Proceedings of the Advances of Science and Technology: 6th EAI International Conference, ICAST 2018, Bahir Dar, Ethiopia, 5–7 October 2018; Springer International Publishing: Berlin/Heidelberg, Germany, 2019; Volume 6, pp. 439–456. [CrossRef]
77. Masoud, A.M.; Pham, Q.B.; Alezabawy, A.K.; El-Magd, S.A.A. Efficiency of geospatial technology and multi-criteria decision analysis for groundwater potential mapping in a Semi-Arid region. *Water* **2022**, *14*, 882. [CrossRef]

78. Dar, T.; Rai, N.; Bhat, A. Delineation of potential groundwater recharge zones using analytical hierarchy process (AHP). *Geol. Ecol. Landsc.* **2021**, *5*, 292–307. [CrossRef]
79. Hagos, Y.G.; Andualem, T.G. Geospatial and multi-criteria decision approach of groundwater potential zone identification in Cuma sub-basin. Southern Ethiopia. *Heliyon* **2021**, *7*, e07963. [CrossRef] [PubMed]
80. Rajesh, J.; Pande, C.B.; Kadam, S.A.; Gorantiwar, S.D.; Shinde, M.G. Exploration of groundwater potential zones using analytical hierarchical process (AHP) approach in the Godavari River basin of Maharashtra in India. *Appl. Water Sci.* **2021**, *11*, 182. [CrossRef]
81. Owolabi, S.T.; Madi, K.; Kalumba, A.M.; Orimoloye, I.R. A groundwater potential zone mapping approach for semi-arid environments using remote sensing (RS), geographic information system (GIS), and analytical hierarchical process (AHP) techniques: A case study of Buffalo catchment, Eastern Cape, South Africa. *Arab. J. Geosci.* **2020**, *13*, 1–17. [CrossRef]
82. Chevalier, L.; Goedhart, M.; Woodford, A.C. *The Influence of Dolerite Sill and Ring Complexes on the Occurrence of Groundwater in Karoo Fractured Aquifers: A Morpho-Tectonic Approach*; WRC Report No. 937/1/01; Water Research Commission: Pretoria, South Africa, 2001; p. 165.
83. Nisar, U.B.; Ehsan, S.A.; Farooq, M.; Pant, R.R.; Khan, N.G.; Qaiser, F.U.R.; Butt, F.M. Integrated Geoelectrical and Geological Investigation of a Quaternary Paleo-Depositional Environment in the Haripur Basin, Northern Pakistan: Implications for Groundwater System. *Geofluids* **2023**, *13*, 1057457. [CrossRef]
84. Murray, R.; Cobbing, J.; Woodford, A.; Ravenscroft, L.; Chevallier, L. *Groundwater Research Needs in the Eastern Karoo Basin of South Africa*; Water Research Commission: Pretoria, South Africa, 2006; p. 52.
85. Abdekareem, M.; Abdalla, F.; Al-Arifi, N.; Bamousa, A.O.; El-Baz, F. Using remote sensing and GIS-based frequency ratio technique for revealing groundwater prospective areas at Wadi Al Hamdh watershed, Saudi Arabia. *Water* **2023**, *15*, 1154. [CrossRef]
86. Tolche, A.D. Groundwater potential mapping using geospatial techniques: A case study of Dhungeta-Ramis sub-basin, Ethiopia. *Geol. Ecol. Landsc.* **2021**, *5*, 65–80. [CrossRef]
87. Nachtergaele, F.; van Velthuizen, H.; Verelst, L.; Wiberg, D.; Henry, M.; Chiozza, F.; Yigini, Y.; Aksoy, E.; Batjes, N.; Boateng, E.; et al. *Harmonized World Soil Database*; version 2.0; Food and Agriculture Organization of the United Nations: Rome, Italy, 2023; p. 69.
88. Pradhan, B. Groundwater potential zonation for basaltic watersheds using satellite remote sensing data and GIS techniques. *Cent. Eur. J. Geosci.* **2009**, *1*, 120–129. [CrossRef]
89. Fawcett, T. An introduction to ROC analysis. *Pattern Recog Lett.* **2006**, *27*, 861–874. [CrossRef]